

Detecting Secular Perturbations in *Kepler* Planetary Systems Using Simultaneous Impact Parameter Variation Analysis (SIPVA)

ZHIXING LIU¹ AND BONAN PU²

¹*College of Letters and Science, University of California, Santa Barbara, Santa Barbara, CA 93106, USA*

²*Independent Researcher, New York, NY 10018, USA.*

ABSTRACT

Recovering impact parameter variations in multi-planet systems is an effective approach for detecting non-transiting planets and refining planetary mass estimates. Traditionally, two methodologies have been employed: the *Individual Fit*, which fits each transit independently to analyze impact parameter changes, and the *Dynamical Fit*, which simulates planetary dynamics to match transit light curves. We introduce a new fitting method, *Simultaneous Impact Parameter Variation Analysis* (SIPVA), which outperforms the *Individual Fit* and is computationally more efficient than the *Dynamical Fit*. SIPVA directly integrates a linear time-dependent model for impact parameters into the Monte Carlo Markov Chain (MCMC) algorithm by fitting all transits simultaneously. We evaluate SIPVA and the *Individual Fit* on artificial systems with varying LLRs and find that SIPVA consistently outperforms the *Individual Fit* in recovery rates and accuracy. When applied to selected *Kepler* planetary candidates exhibiting significant transit duration variations (TDVs), SIPVA identifies significant impact parameter trends in 10 out of 16 planets. In contrast, the *Individual Fit* does so in only 4. We also employ probabilistic modeling to calculate the theoretical distribution of planets with significant impact parameter variations across all observed *Kepler* systems and compare the distribution of recovered candidates by the *Individual Fit* and *Dynamical Fit* from previous work with our theoretical distribution. Our findings offer an alternative framework for analyzing planetary transits, relying solely on Bayesian inference without requiring prior assumptions about the planetary system's dynamical architecture.

Keywords: Exoplanets, Transit photometry, Impact Parameter Variation, Transit Duration Variation, Markov Chain Monte Carlo, Orbital Dynamics

1. INTRODUCTION

Accurately estimating the mass and eccentricity of exoplanets remains a significant challenge in detecting and characterizing *Kepler* multi-planet systems. One common approach involves reproducing observational data through N-body simulations to determine planetary masses (Wisdom & Holman 1991; Chambers 1999; Doyle et al. 2011; Carter et al. 2012), which has contributed multiple measurements for *Kepler* systems. Despite advancements in numerical integrators (Rein & Liu 2012; Rein & Spiegel 2014; Rein & Tamayo 2015; Rein et al. 2019a,b; Javaheri et al. 2023) and increased computational capabilities, this method is limited by the *Kepler* mission's approximately four-year observational

window, which is insufficient to capture the frequent yet subtle orbital parameter changes necessary for precise mass determination using N-body techniques.

Transit Timing Variation (TTV) analysis is an effective method for estimating exoplanet masses (Agol et al. 2005; Grimm et al. 2018; Dai et al. 2023; Masuda et al. 2024). Several tools, including `ttvim` (Nesvorný & Beaugé 2010), `TTVFast` (Deck et al. 2014), `TTVFaster` (Agol & Deck 2016a), `PhoDyMM` (Jones et al. 2022), and `PyDynamicalC` (Yoffe et al. 2021), facilitate efficient TTV analyses. In addition to mass, studies focusing on eccentricities have examined the fundamental TTV modes to higher orders (Lithwick et al. 2012; Agol & Deck 2016b; Hadden & Lithwick 2017). However, TTV analysis is challenged by mass and eccentricity degeneracies (Lithwick et al. 2012), complicating the precise determination of each individual parameter. Moreover, the limited number of transit observations for planets with shorter orbital periods reduces temporal resolution,

making the detection and analysis of subtle TTV signals more difficult.

Transit Duration Variation (TDV) analysis, especially when combined with TTV, can help overcome the mass-eccentricity degeneracy (Agol & Fabrycky 2018). Recent studies have actively explored using TDVs to constrain exoplanetary parameters (Shahaf et al. 2021; Judkovsky et al. 2020). Physical evidence for secular changes in TDVs driven by variations in impact parameters resulting from mutual inclinations has been presented by Millholland et al. (2021). Consequently, analyzing impact parameter variations (TbVs) has emerged as an alternative approach. Using TbVs, Judkovsky et al. (2022a) analyzed 54 systems with 140 planets, achieving mass detections of more than 3σ for 102 planets, including 43 lighter than $5, M_{\oplus}$. Their subsequent research, Judkovsky et al. (2024), estimates orbital parameters for 101 planets across 23 systems, with mass significances better than 3σ for 95 planets, including 46 without prior constraints.

Recovering and precisely estimating the magnitude and direction of TDVs or TbVs is crucial before using them to constrain planetary parameters. Traditionally, two methodologies have been employed: the *Individual Fit*, which fits each transit independently to analyze TDVs (Holczer et al. 2016), and the *Dynamical Fit*, which simulates planetary dynamics to match transit light curves (Judkovsky et al. 2022a,b, 2024; Langford & Agol 2024).

However, the *Dynamical Fit* requires strong prior assumptions about planetary orbital configurations, including the number of planets, their masses, and gravitational interactions. This research presents a Bayesian inference approach with less assumptions, fitting each planet’s transits individually and independently of neighboring planets. Our method, the *Simultaneous Impact Parameter Variation Analysis* (SIPVA), directly incorporates a linear time-dependent model for impact parameters into the Markov Chain Monte Carlo (MCMC) algorithm by fitting all transits simultaneously. SIPVA avoids modeling the full gravitational dynamics, reducing computational complexity and dependence on prior knowledge of the system’s architecture. We demonstrate that SIPVA outperforms the *Individual Fit* in recovery rate and accuracy, providing an alternative approach for analyzing planetary transits.

This paper is organized as follows. In Section 2, we present a theoretical calculation of the Log Likelihood Ratio (LLR) of TbV transit lightcurves between the Null Model (\mathcal{M}_0), which assumes no change in the impact parameter over time, and the Alternative Model (\mathcal{M}_1), which incorporates a changing impact parameter. In

Section 3, we introduce our MCMC methodology for recovering impact parameter changes through both *Individual Fits* (Sections 3.2 and 3.3) and SIPVA after transit folding (Section 3.4). We also evaluate the performance of *Individual Fits* and SIPVA on various artificial systems with different LLRs (Section 3.5). Section 4 applies our fitting algorithms to the selected *Kepler* planetary system candidates from Millholland et al. (2021) that demonstrate significant TDV. Lastly, in Section 5, we develop a theoretical model to estimate the relative frequency of planets exhibiting significant impact parameter changes across all *Kepler* observations and compare our estimates with observations from Holczer et al. (2016) and Judkovsky et al. (2022a, 2024). Finally, in Section 6, we summarize our findings.

For clarity, we have provided a notation table (Table 1) summarizing the variables used throughout this paper.

2. THEORETICAL LOG-LIKELIHOOD RATIO

To evaluate the detectability of impact parameter variations due to secular perturbations in multi-planet systems, we derive the theoretical log-likelihood ratio (LLR) between two models: the Null Model (\mathcal{M}_0), which assumes no change in the impact parameter over time, and the Alternative Model (\mathcal{M}_1), which incorporates a changing impact parameter. The log-likelihood ratio (LLR) between these models is defined as:

$$\text{LLR} = 2(\ln \mathcal{L}_1 - \ln \mathcal{L}_0), \quad (1)$$

where \mathcal{L}_1 and \mathcal{L}_0 are the likelihoods of the data under models \mathcal{M}_1 and \mathcal{M}_0 , respectively.

To compute the LLR in this context, we model the flux difference resulting from a small change in the impact parameter. During a planetary transit, the observed flux decrease can be modeled using the analytical expressions provided by Mandel & Agol (2002). For a transit without limb darkening, the flux is given by:

$$F(z) = 1 - \frac{1}{\pi} \left(p^2 \kappa_0 + \kappa_1 - \sqrt{\frac{4z^2 - (1 + z^2 - p^2)^2}{4}} \right), \quad (2)$$

where $p = r_p/r_*$ is the planet-to-star radius ratio, and $z = d/r_*$ is the normalized center-to-center distance between the star and planet. The auxiliary functions κ_0 and κ_1 are defined as:

$$\kappa_0 = \cos^{-1} \left(\frac{p^2 + z^2 - 1}{2pz} \right), \quad (3)$$

$$\kappa_1 = \cos^{-1} \left(\frac{1 - p^2 + z^2}{2z} \right). \quad (4)$$

Table 1. Notation Table

Notation	Description	Notation	Description
t	Time	T	Period
a	Semi-major axis	p	Planet-star radius ratio
b	Impact parameter	u_1	Limb darkening parameter 1
R_*	Radius of the star	u_2	Limb darkening parameter 2
M_*	Mass of the star	ρ_*	Stellar density (g/cm ³)
m	Mass of the planet	ω	Orbital frequency
δ_t	Time interval of short-cadence of Kepler	n	Number of data points
t_e	Transit epoch	N	Number of planets in the system
\dot{b}	Change in impact parameter over time	N_T	Number of transits
\hat{b}_{ind}	Estimate of \dot{b} from <i>Individual Fit</i>	\hat{b}_{grp}	Estimate of \dot{b} from SIPVA
$t_{\hat{b},\text{ind}}$	t-value of \hat{b} from <i>Individual Fit</i>	$t_{\hat{b},\text{grp}}$	t-value of \hat{b} from SIPVA
z	Normalized separation between centers	\bar{F}	Raw flux from Kepler
\hat{F}	Model flux from $\bar{\Theta}$	F	Actual flux from Kepler
σ	Standard deviation for error in F and \hat{F}	σ_I	Standard deviation for inclination
secw	$\sqrt{e} \cos \omega$	sesw	$\sqrt{e} \sin \omega$
$q1_{\text{Kepler}}$	Limb darkening coefficient 1 (Kepler)	$q2_{\text{Kepler}}$	Limb darkening coefficient 2 (Kepler)
$\log_{10}(\sigma_{\text{wn}})$	Log white noise standard deviation		

NOTE—This table summarizes the notation and variables used throughout this paper.

This model is valid within the range $|1 - p| < z < 1 + p$. The separation z depends on the impact parameter b and the position along the transit chord x , such that $z = \sqrt{b^2 + x^2}$. The impact parameter b represents the projected distance between the centers of the star and planet at mid-transit, normalized by the stellar radius.

To assess the effect of a small change in the impact parameter over the observational period, we consider a linear variation $\Delta b = \dot{b} N_T T$, where \dot{b} is the rate of change of the impact parameter, N_T is the number of observed transits, and T is the orbital period. The flux difference resulting from this change can be approximated using a first-order Taylor expansion:

$$\delta F(x, b) = F(x, b + \Delta b) - F(x, b) \approx \frac{\partial F(x, b)}{\partial b} \Delta b. \quad (5)$$

The mean squared flux difference over the transit is then:

$$\langle (\delta F)^2 \rangle = \frac{1}{2(1+p)} \int_{-(1+p)}^{(1+p)} \left[\frac{\partial F(x, b)}{\partial b} \Delta b \right]^2 dx. \quad (6)$$

Assuming Gaussian noise with variance σ_b^2 in the flux measurements, the theoretical log-likelihood ratio between the models with and without impact parameter change is:

$$\begin{aligned} \text{LLR}^2 &= \sum_{i=0}^n \frac{(F_{\mathcal{M}_1}(z_i) - F_{\mathcal{M}_0}(z_i))^2}{\sigma_b^2} \\ &= \langle \delta F^2 \rangle \left(\frac{\tau}{\delta_t} \right) \frac{1}{2\sigma_b^2}, \end{aligned} \quad (7)$$

where τ is the total duration of observations, δ_t is the time interval between measurements (e.g., *Kepler*'s short cadence of 2 minutes), and $n = \tau/\delta_t$ is the total number of data points collected. The term $\langle (\delta F)^2 \rangle$ quantifies the average squared flux difference due to the impact parameter change over the transit.

The fiducial value for $\sigma_b = 3.88 \times 10^{-4}$ is estimated as follows. We start with a baseline noise level of $\sigma = 1 \times 10^{-4}$ (or 100 ppm), which is representative of the noise levels observed among solar-type stars in the Kepler field of view. According to Gilliland et al. (2015), approximately 38% of stars have noise levels below 70 ppm, indicating that the median noise level is slightly above this threshold. To obtain a more realistic effective noise value for our aggregated data, we account for the increase in noise when converting from the 30-minute long cadence to the 2-minute short cadence of the Kepler data. Specifically, we multiply the baseline noise by $\sqrt{15}$, since there are 15 short-cadence measurements within each long-cadence interval (30min/2min = 15). This yields $\sigma_b = \sigma \times \sqrt{15} \approx 3.88 \times 10^{-4}$.

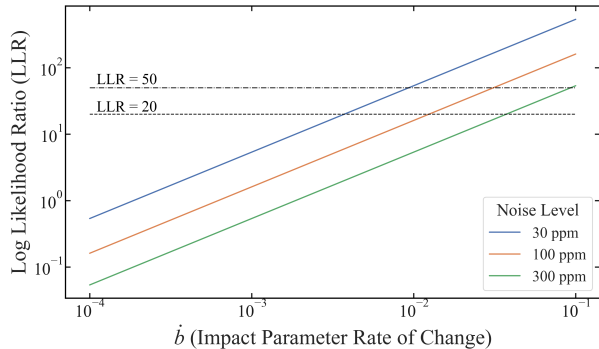


Figure 1. The variation of the Log Likelihood Ratio (LLR) as a function of the impact parameter rate of change \dot{b} (see Table 1 for variable definitions), for three noise levels: 30 ppm, 100 ppm, and 300 ppm. The x -axis shows \dot{b} , ranging from 10^{-4} to 10^{-1} , while the y -axis displays the corresponding LLR values. This calculation assumes a planet star radius ratio $p = 0.01$, impact parameter $b = 0.5$, orbital period $T = 30$ days, and 50 observed transits. Dashed lines are shown at $\text{LLR} = 20$ and $\text{LLR} = 50$, indicating the thresholds at which the SIPVA and the *Individual Fit* method can recover the impact parameter change, respectively. Further details on the significance of these thresholds are provided in Section 3.5.

In Figure 1, we present the variation of the Log Likelihood Ratio (LLR) as a function of the impact parameter rate of change, \dot{b} , for three noise levels: 30 ppm, 100 ppm, and 300 ppm. The x -axis represents \dot{b} , ranging from 10^{-4} to 10^{-1} , and the y -axis shows the corresponding LLR values. For the LLR calculation, we assume a planet-star radius ratio $p = 0.01$, an impact parameter $b = 0.5$, an orbital period $T = 30$ days, and 50 observed transits. Dashed lines are plotted at $\text{LLR} = 20$ (indicating the threshold where SIPVA, can recover the impact parameter change) and $\text{LLR} = 50$ (representing the point at which the *Individual Fit* method can recover the impact parameter change). Further discussion of the significance of these LLR thresholds is provided in Section 3.5.

When the noise level is 30 ppm, the LLR reaches 20 when \dot{b} is $3.7 \times 10^{-3} \text{yr}^{-1}$ and 50 when \dot{b} increases to $9.3 \times 10^{-3} \text{yr}^{-1}$. However, if the noise level increases to 100 ppm, the LLR reaches 20 when \dot{b} is 0.0124yr^{-1} , and 50 when \dot{b} equals 0.031yr^{-1} . Lastly, with a noise level as high as 300 ppm, \dot{b} must reach 0.037yr^{-1} for the LLR to be 20, and 0.093yr^{-1} for the LLR to reach 50. The \dot{b} value of 0.093yr^{-1} is extremely unlikely to occur, as discussed in the later section on the relative frequency of \dot{b} (see Section 5).

Under typical noise conditions (100 ppm), our analysis shows that \dot{b} must exceed 0.0124yr^{-1} to be detectable by SIPVA ($\text{LLR} = 20$). This aligns with the findings of

Judkovsky et al. (2024), on the typical detectable TbV rates are on the order of 10^{-2}yr^{-1} .

3. METHODOLOGY

In this section, we present our methodologies for detecting changes in impact parameters from planetary transits using MCMC techniques: the *Individual Fit* and the SIPVA. Section 3.1 uses Monte Carlo simulations to generate artificial light curves with various log-likelihood ratios. Sections 3.2 and 3.3 detail the approach of independently fitting each transit using MCMC, referred to as the *Individual Fitting* method. In Section 3.4, we introduce the SIPVA method. Here, we explain how we incorporate the assumption of a linear time-dependent impact parameter directly into the MCMC framework by folding the transits and outlining the method for quantifying inter-transit uncertainty. Section 3.5 evaluates the effectiveness of the *Individual Fitting* and SIPVA methods by examining the recovery rates at various log-likelihood ratios, assessing the accuracy of recovered impact parameter estimations using percentage differences, and analyzing the areas under the Receiver Operating Characteristic (ROC) curves. Finally, Section 3.6 summarizes the assumptions and the number of parameters used in the *Individual Fit*, *Dynamical Fit*, and SIPVA methods, providing a comparative overview of their methodologies.

3.1. Generating Artificial System Based on Log Likelihood Ratio

Using Monte Carlo simulations, we generate artificial light curves for exoplanets with varying LLRs, with initial conditions selected from uniform distributions. These include impact parameters ranging from 0.07 to 0.5, planet-star radius ratios from 0.001 to 0.1, impact parameter rate of change from 0.01 to 0.03 per year, star radius to semi-major axis ratios from 1/30 to 1/100, and the number of transits from 30 to 100. The orbital period of each planet is calculated by dividing four years by the number of transits. In the final step, we filter systems to ensure they are physically plausible by calculating the stellar density from the scaled semimajor axis (ratio of the semi-major axis to the stellar radius) and the orbital period. We only consider systems whose stellar density falls within the range of 0.1 to 10 gram per cubic centimeter.

We calculate LLRs using the formula presented in Section 2, filtering for a 1% tolerance to isolate specific LLR values: 5, 10, 15, 20, 30, 50, and 100.

Lastly, we simulate light curves for these parameters using PyTransit (Parviainen 2015), adding noise from a normal distribution with a standard deviation of 10^{-4}

(Gilliland et al. 2015) to model realistic observational data.

3.2. Initial Transit Fitting Approach

We begin by fitting each transit separately, using the MCMC process, with the light curve computed with `PyTransit` and MCMC implemented with `emcee` (Foreman-Mackey et al. 2013).

We use distinct transit epochs as priors for each transit, acknowledging that each transit occurs differently. The transit epoch priors are determined by the median time of each transit with an uncertainty of 0.5 d. However, we maintain consistent prior means and uncertainties for other stellar parameters, such as the period and stellar density, across all transits, based on the assumption that the same planet orbits the same star.

Given that we generate the light curves ourselves, we know their true parameters. We introduce a degree of uncertainty to prevent giving our analysis an unfair advantage by using these exact parameters as priors. This is accomplished by applying normal variations to the true values, setting the standard deviation for these perturbations at 1% for both the orbital period and the planet-star size ratio, 5% for the impact parameter, and 10% for the stellar density. We assume the star's flux can be approximated by the quadratic limb darkening model proposed by Mandel & Agol (2002). The change in the star's flux due to transiting planets can be calculated using the impact parameter b and the parameter vector $\vec{\Theta}$, defined as

$$\vec{\Theta} = \langle t_e, T, p, \rho, \text{secw}, \text{sesw}, q1_{\text{Kepler}}, q2_{\text{Kepler}}, \log_{10}(\sigma_{\text{wn}}) \rangle, \quad (8)$$

where t_e denotes the transit midtime. T represents the planet's orbital period, and the planet star radius ratio, p , is derived from the square root of the transit depth, indicating the planet's star area ratio. The stellar density, ρ_* , is expressed in grams per cubic centimeter units. The terms `secw` and `sesw` control the eccentricity and orientation of the orbit through $\sqrt{e} \cos \omega$ and $\sqrt{e} \sin \omega$, respectively. The quadratic limb darkening coefficients, $q1_{\text{Kepler}}$ and $q2_{\text{Kepler}}$, account for the variation in brightness as the planet transits across the star's disk in the Kepler passband. Finally, $\log_{10}(\sigma_{\text{wn}})$ quantifies the average white noise standard deviation for the first light curve, expressed in logarithmic form.

The log-likelihood function for the j th transit, $\ell_j(\vec{\Theta}, b | F_j, \sigma_j)$, is formulated based on the observed flux F_j and the calculated flux $\hat{F}_j(\vec{\Theta}, b)$, as shown in the equation:

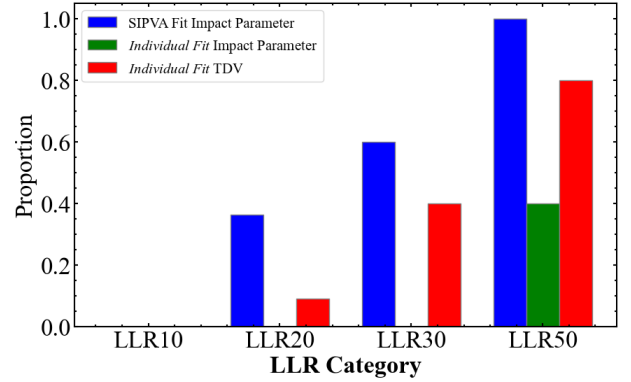


Figure 2. Relative proportion of significant t-values indicating successful recovery of impact parameter changes for different Log Likelihood Ratio (LLR) categories. The blue bars represent SIPVA Fit impact parameters, the green bars represent *Individual Fit* of impact parameters, and the red bars represent *Individual Fit* of Transit Duration Variation (TDV). The x-axis categorizes the systems based on their LLR values (10, 20, 30, and 50), and the y-axis represents the proportion of systems within each LLR category for which the t-value exceeded the threshold of 3, indicating a successful recovery.

$$\ell_j(\vec{\Theta}, b | F_j, \sigma_j) = - \sum_{t=0}^n \frac{(F_j(t) - \hat{F}_j(\vec{\Theta}, b, t))^2}{2\sigma_j^2} - \frac{1}{2} \log \sigma_j^2 \quad (9)$$

For the j th transit, we assume the standard deviation of white noise, σ_j , to be a constant at 1×10^{-4} . The logarithmic posterior distribution of parameters $\vec{\Theta}$ and b , based on the observed flux F_j , integrates both the prior knowledge and the likelihood of observing F_j given $\vec{\Theta}$ and b . This relationship is mathematically expressed as:

$$\log P(\vec{\Theta}, b | F_j) = -\frac{1}{2} \left(\sum_{i=1}^8 \left(\frac{\vec{\Theta}_i - \mu_{\vec{\Theta}_i}}{\sigma_{\vec{\Theta}_i}} \right)^2 + \left(\frac{b - \mu_b}{\sigma_b} \right)^2 \right) + \log(2\pi\sigma_{\vec{\Theta}_i}^2) + \log(2\pi\sigma_b^2) + \ell_j(\vec{\Theta}, b | F_j), \quad (10)$$

note that we drop σ_j dependence as this term is assumed to be constant for the current stage.

Parameter estimates for each transit are derived from the posterior distribution's median (50th percentile). The uncertainties are determined by comparing the upper error (86th percentile minus the median) and the lower error (median minus the 14th percentile) and taking the greater of these values.

3.3. Second Phase of Transit Fitting

In the second phase of transit fitting, we refine our analysis by using the posterior parameters and their uncertainties from the initial fit as priors for a subsequent fit. This involves compiling the estimates and uncertainties from all prior transits, selecting the median as the system’s overall parameter estimate, and choosing the median of the uncertainties as the overall uncertainty. The refined estimates and their uncertainties are then employed as priors for the next fitting stage to enhance the accuracy of our parameter determinations. The second fitting round is necessary because the initial priors, based on previous research, may have different model assumptions.

After completing the second fitting, we record the median values and their uncertainties. We then perform a weighted linear regression on the posterior impact parameter estimates relative to each transit’s timing, using the uncertainties as weights. The slope from this regression estimates the rate of change in the impact parameter. Additionally, we perform a weighted linear regression of transit durations against their timings, using the resulting coefficients as another indicator of impact parameter variations.

3.4. Simultaneous Impact Parameter Variation Analysis

Lastly, we fit all transits simultaneously, employing the MCMC method as before. The median values from the second fitting round serve as our initial priors mean and uncertainty.

A critical step in this final stage involves temporally aligning all transits, a technique often referred to as “folding” the transits. To achieve this, we first determine each transit’s midpoint, t_j , by re-analyzing them using their respective posterior median values from the second phase, but this time incorporating 10^6 data points for enhanced precision. The transit mid-times, t_j , are identified by the moments when the flux magnitude reaches its minimum. We then shift each transit by $t_j - t_0$ to ensure all transits are simultaneous. We also document the time difference, $t_j - t_0$, denoted as τ_j . By setting the occurrence time of the first transit, t_0 , to zero, τ_j also defines the epoch for each subsequent transit.

We develop a combined likelihood function, \mathcal{L} , for evaluating all transit together. This approach is based on the assumption that the impact parameter changes linearly throughout the observation period. Therefore, we can estimate the impact parameter for any transit, b_j , starting from the first transit’s impact parameter, b_0 , and adjusting for time as follows:

$$b_j = b_0 + \dot{b}\tau_j \quad (11)$$

Here, \dot{b} means the rate of change of the impact parameter over time, measured in years.

Consequently, the combined log-likelihood function, $\mathcal{L}(\vec{\Theta}, b_0, \dot{b} | \tau_j, \sigma_j F)$, sums up the likelihoods of each individual transit (see Table 1 for definitions of b_0, \dot{b} , and other parameters), $\ell_j(\vec{\Theta}, b_j | F_j, \sigma_j)$, with the impact parameter for each b_j calculated based on our linear time adjustment:

$$\begin{aligned} \mathcal{L}(\vec{\Theta}, b_0, \dot{b} | \tau_j, F, \sigma_j) &= \sum_{j=1}^{N_T} \ell_j(\vec{\Theta}, b | F_j, \sigma_j) \\ &= \sum_{j=1}^{N_T} \sum_{t=0}^n \frac{(F_j(t) - \hat{F}_j(\vec{\Theta}, b, t))^2}{2\sigma_j^2} \\ &\quad - \frac{1}{2} \sum_{j=1}^{N_T} \log \sigma_j^2. \end{aligned} \quad (12)$$

The current log-likelihood function operates under the assumption that all transits contribute equally to the final estimation, maintaining a constant σ_j across all transits. However, in *Individual Fits*, we address inter-transit variations by incorporating the uncertainty from the posterior estimation of the impact parameter into the linear regression. In the SIPVA, we adopt a similar approach by computing the relative uncertainty, σ_j , for each transit, from the root mean square deviation (RMSE):

$$\sigma_j = \sqrt{\frac{\sum_{t=0}^n (F_j - \hat{F}_j(\vec{\Theta}, b_j, t))^2}{n}} \quad (13)$$

This equation computes σ_j by averaging the absolute differences between the observed and simulated fluxes over the data points within transit j , where n represents the number of data points within transit j .

We then use differential evolution to obtain the Maximum Likelihood Estimates of σ_j of each transit by maximizing the expression

$$S(\vec{\Theta}, b_0, \dot{b}) = \sum_{j=1}^{N_T} \log \sum_{t=0}^n \frac{(F_j(t) - \hat{F}_j(\vec{\Theta}, b_j, t))^2}{n} \quad (14)$$

to get the tentative estimates of $\vec{\Theta}, b_0$, and \dot{b} . Subsequently, these estimates are utilized to reconstruct the flux for each transit and compare it with the observed flux. Therefore, the uncertainty of each transit σ_j , is derived by using the estimates of $\vec{\Theta}, b_0$, and \dot{b} at equation 13.

To prevent overfitting, we set the prior for the rate of change of the impact parameter, \dot{b} , to zero. The initial impact parameter, b_0 , is assigned a prior mean and uncertainty based on the intercept’s best estimate and uncertainty from the linear regression analysis. Since we’ve aligned all transits to have their centers at zero, we set the prior for the transit epoch to zero with a small uncertainty of 1×10^{-5} days. This tight uncertainty is justified because we generated one million (1×10^6) data points, and transit durations are typically up to 10 days. For the other parameters, we select priors based on the median of all transits’ posterior medians and their uncertainties.

Therefore, the posterior distribution of parameter vector $\vec{\Theta}$, initial impact parameter b_0 , and changing of impact parameter \dot{b} given the transit epoch of each transit τ_j , relative uncertainty of each transit σ_j , and observation flux of all transit F , can be derived as

$$\log P(\vec{\Theta}, b_0, \dot{b} | \sigma_j, \tau_j, F) = \mathcal{L}(\vec{\Theta}, b_0, \dot{b} | \tau_j, F, \sigma_j) + Q(\vec{\Theta}, b_0, \dot{b}) \quad (15)$$

where $Q(\vec{\Theta}, b_0, \dot{b})$ represents the quadratic penalty for deviations of the parameters $\vec{\Theta}, b_0, \dot{b}$ from their prior means, scaled by their prior standard deviations. This penalty term can be written as:

$$Q(\vec{\Theta}, b_0, \dot{b}) = -\frac{1}{2} \left(\sum_{i=1}^8 \left(\frac{\vec{\Theta}_i - \mu_{\vec{\Theta}_i}}{\sigma_{\vec{\Theta}_i}} \right)^2 + \left(\frac{b_0 - \mu_{b_0}}{\sigma_{b_0}} \right)^2 + \left(\frac{\dot{b} - \mu_{\dot{b}}}{\sigma_{\dot{b}}} \right)^2 \right) - \log \left(2\pi \sigma_{\vec{\Theta}_i}^2 \sigma_{b_0}^2 \sigma_{\dot{b}}^2 \right) \quad (16)$$

In SIPVA, we implicitly assume that limb darkening coefficients (LDCs) remain constant over the 3-4 years of observations. This assumption is justified since LDCs depend on fundamental stellar properties such as effective temperature (T_{eff}), surface gravity ($\log g$), and metallicity ($[M/H]$), which typically do not change significantly over short timescales for most stars (Claret & Bloemen 2011; Sing 2010). Model-based LDCs derived from ATLAS stellar atmosphere grids (Castelli & Kurucz 2003) have been shown to align well with observational data, ensuring their reliability without requiring frequent recalculations. Additionally, stellar atmospheres are stable over such periods, leading to consistent intensity distributions across the stellar disk. Studies of the Sun—our closest stellar proxy—have shown

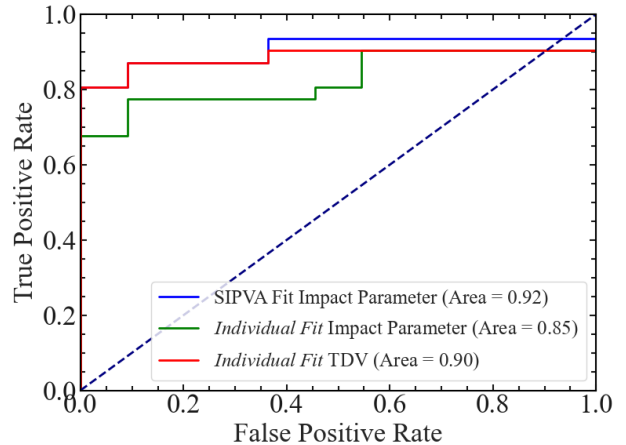


Figure 3. ROC curves comparing true positive rates to false positive rates for SIPVA impact parameters (blue line), *Individual Fit* impact parameters (green line), and *Individual Fit* Transit Duration Variation (TDV) (red line). The area under the curve (AUC) for each method indicates effectiveness: SIPVA (AUC = 0.92), *Individual Fit* of impact parameters (AUC = 0.85), and *Individual Fit* of TDV (AUC = 0.90). The diagonal dashed line represents a random guess.

that limb darkening coefficients remain relatively constant over short periods, with notable changes occurring only over longer solar cycles of about 11 years (Moon et al. 2017). Therefore, assuming constant LDCs throughout the *Kepler* mission simplifies the analysis without significantly affecting accuracy.

3.5. Results

We applied both *Individual Fits* and SIPVA to ten systems with LLRs of 10, 20, 30, and 50. Systems with an LLR of 10 or below were categorized as having no discernible signal. Successful recovery of impact parameter changes was defined as instances where the t-value—calculated as the ratio of the estimation to the uncertainty—exceeded 3.

Figure 2 presents a bar graph summarizing the proportion of successful recoveries for each method across different LLRs. The SIPVA and *Individual Fit* TDV methods partially recover the Impact Parameter Variation Signal when the LLR is greater than or equal to 20. The *Individual Fit* impact parameter recovers its variation when the LLR is greater than or equal to 50. SIPVA consistently outperforms the *Individual Fit* (TDV and impact parameter) methods at all tested LLR levels in terms of recovery proportion.

Both the SIPVA and *Individual Fit* TDV methods require a Log-Likelihood Ratio (LLR) close to 20 to recover the impact parameter variation successfully. We define recovery as achieving a t-score greater than 3 ($t_{b,\text{grp}} > 3$). Since the LLR is related to the square

of the t-score (see proof in Appendix A), an LLR exceeding 9 should suffice to reach a t-score of 3. However, our derivation in Appendix A does not account for the simultaneous changes in estimating other parameters when including \dot{b} in the model. Correlations between these parameters can inflate uncertainties in \dot{b} , requiring a stronger signal (higher LLR) to achieve the same t-score.

Additionally, since SIPVA operates within a Bayesian inference framework, the uncertainties in the priors may influence the recovery rate. In Section 3.4, we assume a linear change in the impact parameter over time, modeling it as $b_j = b_0 + \dot{b}\tau_j$, and to prevent overfitting, we set the prior for \dot{b} to zero with a relatively tight uncertainty, effectively constraining its possible values. This conservative prior makes detecting small variations in b more challenging, necessitating a higher LLR to overcome the prior constraint. Similarly, as outlined in Section 3.2, the priors for other parameters are also perturbed to introduce realistic uncertainties: 1% for the orbital period and planet-star radius ratio, 5% for the impact parameter, and 10% for the stellar density. These perturbations, reflecting uncertainties inherent in real observational data, contribute additional sources of uncertainty, further increasing the required LLR to approach 20 for achieving a t-score greater than 3.

To further assess the performance of our methods, we employed ROC curves, illustrated in Figure 3. ROC curves plot the true positive rate (sensitivity) against the false positive rate (1 minus specificity) for various threshold settings, thereby illustrating the diagnostic ability of each method. In this study, ROC curves enable us to evaluate how well the *Individual Fits* and SIPVA distinguish between systems with and without significant impact parameter variations across different LLRs. By analyzing the area under the ROC curve (AUC), we quantitatively compared the effectiveness of the methods. The results reveal that SIPVA achieves a larger AUC compared to the individual methods, indicating better overall performance in identifying true positives while minimizing false positives.

An interesting observation is that the *Individual Fit* method performs better when analyzing TDVs than impact parameter changes. This discrepancy can be understood by examining the relationship between the transit duration rate of change and various orbital parameters. According to Equation (4) of Millholland et al. (2021), the time derivative of the transit duration is given by:

$$\dot{T}_{\text{dur}} = -T_{\text{dur}} \left[\dot{b} \frac{b}{(1-b^2)} + \frac{\dot{v}_{\text{mid}}}{v_{\text{mid}}} \right], \quad (17)$$

where T_{dur} is the transit duration, b is the impact parameter, v_{mid} is the orbital velocity at mid-transit, and the dots denote time derivatives. This equation suggests that \dot{T}_{dur} depends not only on changes in the impact parameter \dot{b} but also on variations in the orbital velocity \dot{v}_{mid} . The orbital velocity changes are influenced by precessional effects related to the longitude of the ascending node (Ω), the argument of periapsis (ω), and the orbital eccentricity (e). TDVs are thus sensitive to these precessional changes, making them particularly responsive to mutual inclinations and orbital interactions within the system. In contrast, direct fitting of the impact parameter captures only the changes in b without accounting for the additional dynamical information provided by \dot{v}_{mid} . Therefore, *Individual Fit* TDV provides a more informative signal about mutual inclinations and the system’s dynamical evolution than *Individual Fit* Impact Parameter Variations alone.

Lastly, we compare the impact parameter variation estimation accuracy from SIPVA and *Individual Fit* using the percentage difference box plot in Figure 4. The box plots show the percentage differences between the estimated and true values of the impact parameter change rate \dot{b} across different Log-Likelihood Ratio (LLR) categories (10, 20, 30, 50). As the LLR increases, both methods display reduced percentage differences, indicating improved estimation accuracy. However, SIPVA significantly reduces percentage differences compared to *Individual Fit*. Although SIPVA initially has a higher percentage difference at LLR = 10, it surpasses *Individual Fit* at all higher LLR values, showing better overall performance as the LLR increases.

The intuition behind this trend is because of their assumptions on the impact parameter variation. SIPVA assumes a linear change in the impact parameter over time. When this assumption holds—typically at higher LLR values where the signal is strong—SIPVA can effectively model the variation, leading to a significant decrease in the percentage difference between the estimated and actual values. However, at lower LLR values, where the signal is weak, and the linear assumption of impact parameter changes does not hold, SIPVA’s performance deteriorates dramatically because it forces a linear model onto noisy data, resulting in significant errors.

In contrast, *Individual Fit* allows the impact parameter to vary independently for each transit without imposing a global trend. This approach means that when the signal is weak (low LLR), the method’s performance remains stable, as it does not impose a potentially incorrect linear model on the data. However, even at higher LLR values, *Individual Fit* does not see a sig-

nificant improvement in performance because it doesn't capitalize on the consistent, linear trend across transits that SIPVA assumes. Consequently, while SIPVA starts with a higher percentage difference at low LLR, its performance improves rapidly as the LLR increases, outperforming *Individual Fit*, which shows a more modest improvement.

Furthermore, we observe that the spread of the percentage differences, as indicated by the interquartile ranges in the box plots, decreases with increasing LLR for both methods. This reduction in variability signifies that the estimates are becoming more accurate and consistent across simulations. Although \dot{b} is not included in the Fisher information matrix, standard errors scale with flux error rather than LLR. The simultaneous increase in both LLR and precision in estimating \dot{b} arises from a confounding variable: the signal strength in the data, influenced by factors such as planet size and transit duration.

Larger planets and longer transit durations produce deeper, cleaner transits, resulting in higher-quality light curves. A stronger signal enhances the clarity of the transit data, enabling more accurate estimation of the impact parameter change rate. Consequently, the standard error of \dot{b} decreases as signal strength increases. Additionally, as shown by Equations 2 and 7, larger planet size (p) and longer transit duration (τ) also contribute to higher LLR values. Selecting systems with larger radii and longer durations effectively selects for lower flux errors, meaning the absolute error in \dot{b} varies with signal strength. Thus, the increase in LLR does not directly cause the decrease in estimation error; instead, both higher LLR and reduced uncertainty in \dot{b} result from improved signal quality. Therefore, the observed decrease in uncertainty with increasing LLR is due to the higher signal-to-noise ratio of systems with higher LLRs.

3.6. Comparison of Methodologies

The *Individual Fit* approach treats each transit as an independent event, allowing both the impact parameter b and the system parameters $\vec{\Theta}$ to vary independently for each transit. This means that for N_T transits, there are N_T sets of $\vec{\Theta}$ and b , effectively treating each transit without assuming any inter-transit correlations.

In contrast, the SIPVA method assumes that certain system parameters remain constant over the four years of observation. Specifically, it assumes that the limb darkening coefficients and other system parameters encapsulated in $\vec{\Theta}$ are constant for all transits. Additionally, SIPVA assumes that the impact parameter changes linearly over time, modeling it as a linear function. How-

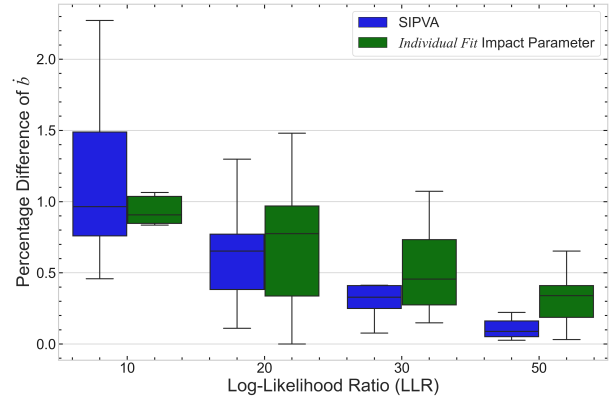


Figure 4. Box plots representing the percentage differences between the estimated and true values of the impact parameter change rate \dot{b} across LLR categories (10, 20, 30, 50) for SIPVA and *Individual Fit*. The x-axis represents the LLR, and the y-axis shows the percentage differences from the true values of \dot{b} . Both methods show lower percentage differences as the LLR increases. The percentage difference of SIPVA decreases more quickly than that of *Individual Fit*. Thus, although SIPVA shows a higher percentage difference at LLR = 10, its percentage difference will be lower at all higher LLR values.

ever, the SIPVA framework is flexible and can accommodate different models for the impact parameter variation, such as a sinusoidal model, which might be appropriate for systems like KOI 142.01 (discussed further in Section 4).

The *Dynamical Fit* methodology by Judkovsky et al. (2022a,b, 2024) operates under several assumptions. Firstly, it assumes that the planetary systems are not in resonance and that all planets have small eccentricities and inclinations. It also assumes that non-secular terms, such as synodic and resonant, depend only on the planets' mean longitudes. Furthermore, similar to SIPVA, *Dynamical Fit* assumes that the limb darkening coefficients remain constant over the four-year observation period and relies on prior research to provide accurate values for these coefficients, as they are not independently fitted in this method. Finally, *Dynamical Fit* assumes that all significant gravitational interactions occur between the transiting planets, which requires prior knowledge of the number of planets in the system to perform N-body simulations.

Regarding the number of parameters in each methodology, the *Individual Fit* method involves $10N_T$ parameters, where N_T is the number of transits. Specifically, there are $9N_T$ parameters for the system parameters $\vec{\Theta}$ and N_T parameters for the impact parameter b , resulting in $9N_T + N_T = 10N_T$ parameters.

For the SIPVA method, the total number of parameters is 11. This includes 9 parameters for the system

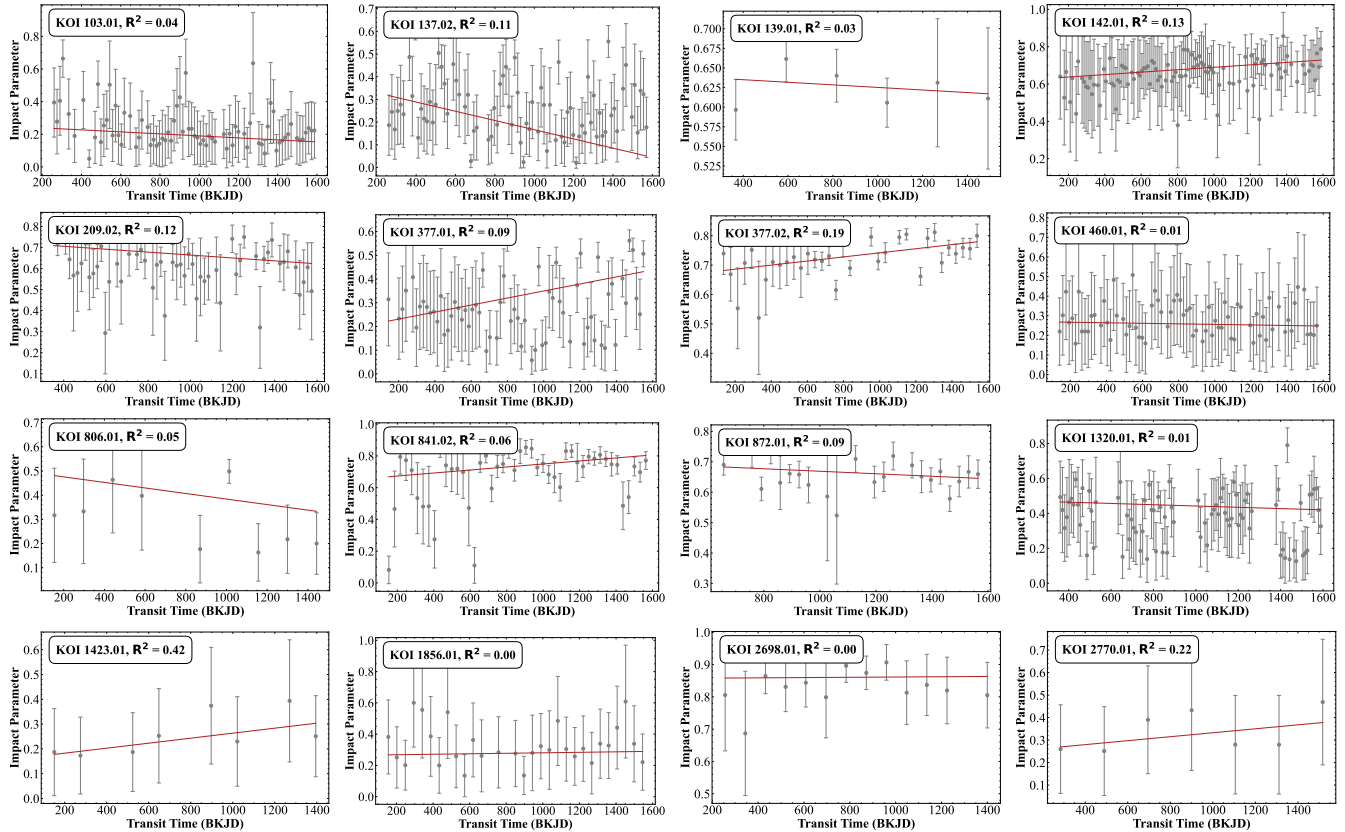


Figure 5. Linear regression of impact parameters from the *Individual Fits* of 16 KOIs exhibiting long-term trends in Transit Duration Variations (TDVs), as selected by Millholland et al. (2021). The x-axis represents the transit midtimes in the Barycentric Kepler Julian Date (BKJD), while the y-axis shows the impact parameters. The t-value (coefficient divided by its uncertainty) and the R-squared value, calculated with weights inversely proportional to the variance of the individual impact parameters, are displayed in the upper left corner of each subplot.

parameters $\vec{\Theta}$, one parameter for the initial impact parameter b_0 , and one parameter for the rate of change of the impact parameter \dot{b} , yielding $9(\vec{\Theta})+1(b_0)+1(\dot{b}) = 11$ parameters.

In the *Dynamical Fit* method, the number of parameters depends on the number of planets in the system. There are 8 parameters per planet, and since all planets in the system are fitted simultaneously, the total number of parameters is $8N$, where N is the number of planets.

4. MODELING KEPLER TRANSITS

Holczer et al. (2016) provided transit depth and duration measurements for 779 Kepler Objects of Interest (KOIs) observed throughout all 17 quarters of the Kepler mission. From this subset, Millholland et al. (2021) identified 16 KOIs showing long-term trends in Transit Duration Variations (TDVs). These KOIs were selected based on three criteria: (1) the fitted TDV slope is greater than three times the slope’s error, (2) the orbital period ranges from 3 to 300 days, and the planetary radius is between 0.5 and 10 Earth radii, and (3) the host stars are part of the cleaned stellar input catalog. We

applied both *Individual Fit* (Sections 3.2 and 3.2) and SIPVA (Section 3.4) techniques to recover changes in the impact parameter for these 16 candidates.

We obtained the light curves of *Kepler* planets from the `lightkurve` database (Lightkurve Collaboration et al. 2018) and supplemented them with existing parameters from the `kplr` database (Foreman-Mackey 2018). To minimize systematic errors in the retrieved physical parameters of exoplanet transits caused by *Kepler*’s long-cadence (LC) data (see Kipping 2010), we prioritized downloading the short-cadence (SC) data when available. The longer integration times of LC data stretch out the ingress and egress durations, suppress limb darkening in the transit trough, and can lead to overestimation of impact parameters—effects that are more pronounced for near-grazing transits where the planet crosses the stellar limb more slowly. This smearing effect also causes an underestimation of stellar density, distorting the inferred physical characteristics of the system. We used the LC data for transits where SC data were unavailable but applied supersampling with

an exposure time of 0.0208 days and a supersampling rate of 15 within the fitting in `PyTransit`.

The light curves were then detrended using the method of [Masuda \(2022\)](#) with the Gaussian Process. For candidates exhibiting TTVs, we downloaded the transit midtimes for KOIs 1320.01, 1423.01, 1856.01, 2698.01, and 2770.01 from [Holczer et al. \(2016\)](#), and for KOIs 377.01 and 377.02 from [Van Eylen & Kjeldsen \(2014\)](#). The remaining candidates, which do not exhibit TTVs, had their transit midtimes calculated using their transit epoch (as provided by the `kplr` database, [Foreman-Mackey 2018](#)) and integer multiples of their orbital period.

The linear regression of impact parameters from the *Individual Fit* is shown in Figure 5. The x-axis represents the transit midtimes, while the y-axis shows the impact parameters. The t-value (coefficient divided by its uncertainty) and the R-squared value are displayed in the upper left corner of each subplot. Each subplot corresponds to the KOI indicated in its subtitle.

Our estimations are summarized in Table 2. The first column lists the KOIs, followed by the second and third columns, which present the estimate of \dot{b} from the *Individual Fit* and its corresponding t-value, $t_{\dot{b},\text{ind}}$. The fourth and fifth columns provide the estimate of \dot{b} from the SIPVA along with its t-value, $t_{\dot{b},\text{grp}}$. The final column, b_0 , indicates the initial impact parameter at the time of the first detected transit, derived from the SIPVA.

The *Individual Fit* identified 4 of the 16 planets with a significant trend in impact parameter changes ($t_{\dot{b},\text{ind}} > 3$), which are KOIs 137.02, 377.01, 377.02, and 841.02. In contrast, the SIPVA detected significant long-term trends in impact parameter changes for 10 of the 16 planets ($t_{\dot{b},\text{grp}} > 3$). For all planets showing significant changes in the SIPVA, the direction of the impact parameter variation aligns with the trends observed in Transit Duration Variation fitting from [Holczer et al. \(2016\)](#). This is consistent, as an increase in Transit Duration Variation over time corresponds to a decrease in the impact parameter.

The SIPVA method failed to recover the impact parameter changes for KOIs 1423.01, 1856.01, 2698.01, and 2770.01 due to the limited number of detrended transits and the strong noise associated with each transit. Additionally, the method was unable to recover the impact parameter changes for KOI 142.01, as its variation is not strictly linear but rather a superposition of a wave-like function and a linear trend, as previously noted by [Nesvorný et al. \(2013\)](#). While KOI 377.01 has multiple clean detrended transits and shows significance in the *Individual Fit* for impact parameters, neither the

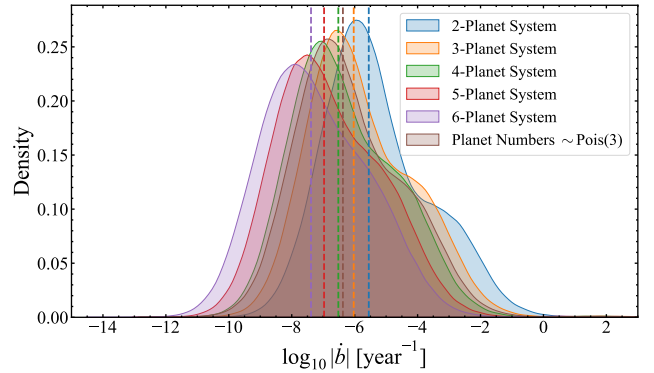


Figure 6. Kernel Density Estimate of the relative frequency of $\log_{10} |\dot{b}|$ for planetary systems with varying multiplicity distributions (see Table 1 for variable definition). The x-axis represents $\log_{10} |\dot{b}|$ (in year^{-1}), where \dot{b} is an orbital dynamical parameter, and the y-axis shows the corresponding relative frequency in the population. Systems with $N = 2$ to 6 planets are based on the model from [Zhu et al. \(2018\)](#), and the Poisson-distributed planet numbers (with $\lambda = 3$) are based on the assumptions from [Lissauer et al. \(2011\)](#). Dashed lines indicate the median of each distribution.

Transit Duration Variation nor the SIPVA for impact parameters revealed a significant long-term trend.

5. MODELING IMPACT PARAMETER VARIATIONS DUE TO MUTUAL INCLINATIONS IN KEPLER PLANETARY SYSTEMS

In this final section, we develop a theoretical model to estimate the relative frequency of planets exhibiting significant impact parameter changes across all *Kepler* observations. This model is based on the physical framework established by [Murray & Dermott \(1999\)](#) and incorporates the inclination distributions derived from [Zhu et al. \(2018\)](#) and [Fabrycky et al. \(2014\)](#). Lastly, we compare the observations of [Holczer et al. \(2016\)](#) and [Judkovsky et al. \(2022a, 2024\)](#) in the context of all discovered Kepler planets, based on the simulation results from our theoretical model (Sections 5.2 and 5.3).

5.1. Theoretical Model

To investigate impact parameter variations (\dot{b}) due to mutual inclinations in multiplanet systems, we derive the relationship between \dot{b} and the rate of change of the mutual inclination $\frac{dI}{dt}$. This relationship is given by (in the limit of small inclinations):

$$\dot{b} \approx \frac{a}{r_*} \left\| \frac{dI}{dt} \right\| \quad (18)$$

where a is the semi-major axis of the planet's orbit, r_* is the radius of the star, and $\left\| \frac{dI}{dt} \right\|$ denotes the magnitude of the rate of change of the mutual inclination.

Table 2. Estimated impact parameter changes (\dot{b}) for Kepler Objects of Interest (KOIs) showing long-term trends in Transit Duration Variations (TDVs)

KOI	$t_{\dot{b},\text{ind}}$	\dot{b}_{ind}	$t_{\dot{b},\text{grp}}$	\dot{b}_{grp}	b_0	T (days)	r (R_{\oplus})
103.01	-1.404	-0.022	-9.735	-0.069	0.496	14.911	2.620
137.02	-6.333	-0.073	-4.350	-0.021	0.418	14.859	5.940
139.01	-0.344	-0.007	-7.284	-0.015	0.657	224.779	7.670
142.01	1.721	0.024	-2.038	-0.005	0.582	10.916	3.930
209.02	-2.263	0.025	-3.165	-0.016	0.489	18.796	7.390
377.01	4.255	0.054	1.129	0.002	0.376	19.271	7.740
377.02	3.541	0.025	12.741	0.010	0.736	38.908	7.980
460.01	-0.252	-0.005	-3.167	-0.048	0.458	17.588	4.030
806.01	-0.877	-0.042	-3.114	-0.038	0.418	143.206	8.900
841.02	3.077	0.035	-4.200	-0.013	0.726	31.330	6.500
872.01	-1.062	-0.013	-6.879	-0.026	0.684	33.601	8.460
1320.01	-1.018	-0.013	3.022	0.005	0.639	10.507	9.010
1423.01	0.683	0.037	-0.454	-0.018	0.157	124.420	10.300
1856.01	0.166	0.006	-0.573	-0.019	0.210	46.299	4.330
2698.01	0.368	0.010	0.225	0.001	0.885	87.972	3.390
2770.01	0.426	0.032	-0.351	-0.015	0.260	205.386	2.110

NOTE—This table summarizes the results of the *Individual Fits* and SIPVA analyses for 16 KOIs exhibiting long-term trends in Transit Duration Variations (TDVs). The KOIs were selected according to the criteria outlined by Millholland et al. (2021). Columns 2 and 3 present the t-value ($t_{\dot{b},\text{ind}}$) and the rate of change in the impact parameter (\dot{b}_{ind}) estimated from the *Individual Fit*. Columns 4, 5, and 6 display the t-value ($t_{\dot{b},\text{grp}}$), the rate of change in the impact parameter (\dot{b}_{grp}), and the initial impact parameter (b_0) obtained from the SIPVA. The last two columns provide the orbital period (T) in days and the planetary radius (r) in Earth radii, both sourced from `kplr` (Foreman-Mackey 2018).

In a system with two planets designated as planet j (inner planet) and planet k (outer planet), the complex inclination I of each planet is represented as $I = \theta e^{i\Omega}$, where θ is the inclination angle, and Ω is the longitude of the ascending node. The rate of change of the mutual inclination between the two planets is given by:

$$\frac{dI_{jk}}{dt} = \omega_{jk} (I_j - I_k) \quad (19)$$

with ω_{jk} is a coupling coefficient that quantifies the strength of the gravitational interaction between the planets. The coupling coefficient is defined as (Murray & Dermott 1999):

$$\omega_{jk} = \frac{Gm_k \alpha b_{3/2}^{(1)}(\alpha)}{4a_j^3 L_j} \quad (20)$$

with G being the gravitational constant, m_k the mass of planet k , a_j the semi-major axis of planet j , L_j the

angular momentum per unit mass of planet j , and $\alpha = a_j/a_k$ the ratio of the semi-major axes.

The Laplace coefficient $b_{3/2}^{(1)}(\alpha)$ arises from the expansion of the disturbing function and is defined by:

$$b_{3/2}^{(n)}(\alpha) = \frac{1}{2\pi} \int_0^{2\pi} \frac{\cos(nt)}{(1 - 2\alpha \cos t + \alpha^2)^{3/2}} dt \quad (21)$$

The angular momentum per unit mass L_j is given by:

$$L_j = m_j \sqrt{GM_* a_j} \quad (22)$$

where m_j is the mass of planet j , and M_* is the mass of the host star. These equations collectively describe how mutual gravitational interactions induce changes in the orbital inclinations and, consequently, the impact parameters of planets in multi-planet systems.

For systems with more than two planets, the rate of change of the inclination for planet j is the sum of the contributions from all other planets:

$$\frac{dI_j}{dt} = \sum_{k \neq j} \omega_{jk} (I_j - I_k) \quad (23)$$

With this theoretical framework established, we proceed to simulate planetary systems to estimate the expected distribution of \dot{b} values, based on the statistics from *Kepler* Planets.

We generate synthetic planetary systems with multiplicities ranging from two to six planets, producing 100,000 systems each. Stellar radii and masses are selected from all confirmed *Kepler* host stars, and planetary radii are drawn from the observed distribution of detected *Kepler* planets.

To estimate the planetary masses, we use the mass-radius relationship from [Zhu et al. \(2018\)](#), assuming an Earth-like composition:

$$\left(\frac{m}{m_{\oplus}}\right) = \left(\frac{r}{r_{\oplus}}\right)^{2.06} \quad (24)$$

where m and r are the planet's mass and radius, respectively, and M_{\oplus} and R_{\oplus} are Earth's mass and radius.

The planets' orbital periods are sampled from the observed *Kepler* period distribution. Additional planets within the same system have periods drawn from a log-uniform distribution to reflect the wide range of orbital configurations observed in exoplanetary systems. The semi-major axes are then calculated using *Kepler*'s third law:

$$a = \left(\frac{GM_* T^2}{4\pi^2}\right)^{1/3} \quad (25)$$

where T is the orbital period of the planet.

The inclination angles are assigned based on a mutual inclination dispersion that depends on the system's multiplicity distribution, N . Following [Zhu et al. \(2018\)](#), we adopt a standard deviation for the inclination distribution given by:

$$\sigma_I = 0.7 \left(\frac{N}{5}\right)^{-4} \quad (26)$$

which suggests systems with more planets tend to have lower mutual inclinations as the increased dynamical interactions lead to more aligned orbits over time ([Becker & Adams 2015](#)).

[Lissauer et al. \(2011\)](#) suggest that a Poisson distribution can model the multiplicity distribution of *Kepler* planets. Furthermore, [Fabrycky et al. \(2014\)](#) indicate that at least half of *Kepler* planets have mutual inclinations consistent with a Rayleigh distribution with a standard deviation of 1 to 2 degrees. Therefore, we introduce an additional simulation where the number of

planets is drawn from a Poisson distribution with a mean of 3 and inclination angles from a Rayleigh distribution with a standard deviation of 2 degrees. Once the number of planets is determined, stellar radii and masses are selected from all confirmed *Kepler* host stars, and planetary radii are drawn from the observed distribution of detected *Kepler* planets, as in the previous simulation.

Figure 6 presents a histogram of \dot{b} , showing the relative frequency for each multiplicity distribution. Dashed lines indicate the medians of each distribution. Table 3 documents the proportion of significant \dot{b} values (defined as $\dot{b} \geq 0.01$) and their relative frequencies within the simulated population. We chose 0.01 as the threshold because [Judkovsky et al. \(2024\)](#) reported that typical detectable TbV rates are on the order of 10^{-2}yr^{-1} .

Naively, systems with more planets should exhibit larger changes in the impact parameter \dot{b} due to increased dynamical orbital interactions. However, our simulations indicate that the significant \dot{b} frequency decreases with higher planet multiplicity. This is evidenced by the median of the relative frequency distribution in Figure 6 gradually shifting to smaller \dot{b} values, and the proportion of significant \dot{b} values decreasing with increasing multiplicity in Table 3. This trend is explained by the dependence of inclination dispersion on the number of planets. According to [Zhu et al. \(2018\)](#), the standard deviation of inclination angles, σ_I , decreases in proportion to the fourth power of planetary multiplicity, as described by Equation 26. For example, a two-planet system has $\sigma_I \approx 27.34^\circ$, while a six-planet system has $\sigma_I \approx 0.34^\circ$, decreasing the inclination dispersion by roughly 80 times.

Smaller mutual inclinations lead to reduced values of $|\dot{b}|$ since \dot{b} is proportional to the differences in inclination and the gravitational coupling between planets. Although the number of pairwise gravitational interactions increases quadratically with the number of planets ($\frac{N(N-1)}{2}$), the strength of each interaction decreases following a fourth-power relationship. Additionally, gravitational perturbations from different planets may partially cancel each other out due to opposing perturbation vectors. Consequently, the decrease in interaction strength dominates the increase in interactions, decreasing the relative frequency of significant \dot{b} values in higher planet multiplicity.

From a stability perspective, systems with more planets naturally adopt lower mutual inclinations to maintain long-term dynamical stability. High mutual inclinations can cause increased gravitational perturbations, orbital crossings, and potential collisions or ejections of planets ([Becker & Adams 2015](#)). Thus, higher-multiplicity systems tend to evolve toward more copla-

nar configurations, reducing the likelihood of significant changes in the impact parameter. This finding is consistent with our simulation results.

5.2. Comparison with *Holczer et al. (2016)*

Holczer et al. (2016) analyzed *Kepler*'s long-cadence light curves and provided transit timing, depth, and duration measurements for 779 *Kepler* Objects of Interest (KOIs) observed over all 17 quarters of the *Kepler* mission. These KOIs were selected based on having transit durations longer than 1.5 hours and signal-to-noise ratios (SNRs) above 10 to ensure reliable duration measurements.

From the TDV catalog compiled by *Holczer et al. (2016)*, *Millholland et al. (2021)* selected 16 KOIs for further study. Their selection criteria included a TDV slope greater than three times its error (indicating a significant TDV trend), planetary radii between $0.5, R_{\oplus}$ and $10, R_{\oplus}$, orbital periods longer than three days, and host stars that are FGK dwarfs included in a clean stellar input catalog.

In contrast, *Shahaf et al. (2021)* used different p -value thresholds to categorize planets based on the significance of linear trends in their transit durations. Planets were classified as having significant TDVs if the p -value was less than 0.001, and as having intermediate significance if $0.001 \leq p\text{-value} < 0.01007$. Notably, *Shahaf et al. (2021)* did not impose any criteria on planet size, orbital period, or host star properties in their sample selection. As a result, they identified 15 KOIs with significant TDVs ($p\text{-value} < 0.001$) and 16 KOIs with intermediate significance.

Our theoretical relative frequency of impact parameter variations (\dot{b}) for various multiplicity distributions is simulated by drawing planetary radii from all observed *Kepler* planets and selecting stellar radii and masses from the pool of confirmed stars. This approach aligns more closely with the selection methodology of *Shahaf et al. (2021)*, who did not restrict their sample based on specific planetary or stellar characteristics. Therefore, we will compare our theoretical relative frequency of \dot{b} with the results reported by *Shahaf et al. (2021)*.

Using data from `kplr` and the radius-mass assumptions from *Zhu et al. (2018)*, our theoretical model for the relative frequency of impact parameter variations predicts the following: 29 planets from two-planet systems, seven planets from three-planet systems, two planets from four-planet systems, half planets from five-planet systems, and no planets from six-planet systems will exhibit significant impact parameter changes.

In comparison, when considering the 15 KOIs with significant TDVs and 16 KOIs with intermediate signif-

icance, a total of 31 planets are classified as having significant TDVs. Among these, 19 KOIs are from single-planet systems, 7 are from two-planet systems, 4 are from three-planet systems, and 1 is from a five-planet system.

Significant changes in the impact parameter are generally unexpected in single-planet systems because no other planets can perturb the planet's orbit gravitationally. The impact parameter should remain stable without such interactions, determined by the orbit's inclination and its alignment relative to the star and observer.

However, *Holczer et al. (2016)* found that 19 *Kepler* KOIs with significant TDVs are in single-planet systems. This discrepancy is consistent with the *Kepler Dichotomy*. Previous studies (*Lissauer et al. 2011*; *Fang & Margot 2012*; *Tremaine & Dong 2012*) identified an excess of single-transiting-planet systems compared to expectations from models with low mutual inclinations. This suggests the existence of two distinct populations: one with nearly coplanar orbits and another with higher mutual inclinations.

In systems with undetected, highly inclined planets, these unseen companions can exert gravitational forces that perturb the observed planet's orbit, causing measurable changes in the impact parameter. Therefore, the significant impact parameter variations observed in single-planet systems may result from interactions with non-transiting, inclined planets that remain undetected due to their orbital geometry.

Another potential explanation involves stellar activity. For instance, if the host star is rapidly rotating, it can become oblate (flattened at the poles), causing deviations from spherical symmetry in its gravitational field. This oblateness can induce slow orbital precession of the planet, altering its impact parameter over long timescales (*Li et al. 2020*). However, the magnitude of the effect caused by stellar oblateness is generally much smaller than that resulting from gravitational interactions with another planet. Therefore, while stellar activity might contribute to impact parameter variations, it is less likely to be the primary cause of significant changes observed in these systems.

The number of planets with significant Transit Duration Variations (TDVs) detected by *Holczer et al. (2016)* is less than what our theoretical model predicts. This discrepancy arises because *Holczer et al. (2016)* selected only 779 *Kepler* Objects of Interest (KOIs) out of 2773 confirmed *Kepler* planets¹ based on criteria such as signal-to-noise ratio and transit duration length. In con-

¹ https://exoplanetarchive.ipac.caltech.edu/docs/counts_detail.html

Table 3. Relative Frequency of Significant \dot{b} in Kepler Systems

Model	Multiplicity Distribution	Relative Frequency (%)
Zhu et al. (2018)	$N = 2$	4.0335
Zhu et al. (2018)	$N = 3$	1.5843
Zhu et al. (2018)	$N = 4$	0.7458
Zhu et al. (2018)	$N = 5$	0.4418
Zhu et al. (2018)	$N = 6$	0.3527
Lissauer et al. (2011)	$N \sim \text{Pois}(3)$	1.0272

NOTE—This table presents the relative frequency of significant rates of change in the impact parameter (\dot{b}) for simulated Kepler planetary systems with varying numbers of planets. The percentages indicate the proportion of planets exhibiting $|\dot{b}| \geq 0.01 \text{ yr}^{-1}$ in our simulations. The decreasing trend in relative frequency with increasing planet multiplicity occurs because higher-multiplicity systems tend to have smaller mutual inclinations to maintain dynamical stability. Consequently, gravitational interactions that contribute to changes in \dot{b} are reduced, leading to fewer instances of significant \dot{b} values in systems with more planets.

trast, our theoretical model is derived from all confirmed planets without such selection criteria. Our model assumes ideal conditions and does not account for uncontrollable observational factors like instrumental noise, data gaps, and observational cadence.

Nevertheless, the overall trend between Holczer et al. (2016)’s findings and our theoretical model shows good agreement: the number of planets exhibiting significant impact parameter changes decreases exponentially as the number of planets in the system increases. This occurs because higher-multiplicity systems tend to have significantly lower inclination dispersions to maintain dynamical stability. The resulting smaller mutual inclinations lead to weaker gravitational interactions between planets, thereby reducing the likelihood of significant changes in the impact parameter.

5.3. Verification With Judkovsky et al. (2022b, 2024)

When comparing our theoretical predictions for the relative frequency of impact parameter changes to observational data, Judkovsky et al. (2022b, 2024) identified 24 planets in two-planet systems, 31 planets in three-planet systems, 43 planets in four-planet systems, and 24 planets in five-planet systems, and five planets in the six-planet systems exhibiting significant transit duration variations (TDVs). After normalizing these numbers by the number of Kepler-discovered planets in each multiplicity category, the relative frequency of planets with significant impact parameters increases with the number of planets in a system. This observed trend contrasts with the inclination distributions reported by Zhu et al. (2018), the relative frequency findings of Holczer et al.

(2016), and the planetary system stability analysis conducted by Becker & Adams (2015), all of which indicate that the relative frequency of planets with significant impact parameter changes decreases as the number of planets in a system increases.

We guess that the discrepancy between our findings and those of Judkovsky et al. (2022b, 2024) may result from potential overfitting in their dynamical models, which tend to emphasize systems with a larger number of planets and complex gravitational interactions. Their photodynamical model, *AnalyticLC* (Judkovsky et al. 2022a), utilizes eight parameters per planet: orbital period, reference mid-transit time, radius ratio, mass ratio, and eccentricity components. Ideally, the observational data should provide sufficient information to constrain these parameters for each additional transiting planet. However, this is not always guaranteed in multi-planet systems. The first few transiting planets typically exhibit the strongest and most easily detectable signals. In contrast, the fourth, fifth, or subsequent planets are often smaller, produce shallower transits, and have lower signal-to-noise ratios. In tightly packed systems, their transits may occur in similar regions of the light curve and over overlapping timescales. While the initial planets significantly influence the inferred system parameters by defining the system’s architecture, additional planets tend to refine these parameters rather than introduce entirely new information, leading to decreased incremental information gains.

This scenario might explain why Judkovsky et al. (2022b, 2024) report solutions with relatively high eccentricities—unusually high values for multi-planet sys-

tems. It suggests their model may stretch parameters to fit the noise associated with the additional planets rather than capture underlying trends. Consequently, the risk of overfitting increases with the number of planets, even though the number of parameters per planet remains constant.

Moreover, it's preferable for the parameters describing the system to be independent. However, as more planets are added, the orbital elements—such as eccentricities and inclinations—can become interdependent across different planets. Changes in one planet's parameters might compensate for changes in another's, producing similar transit signals and complicating the unique determination of each planet's parameters. Judkovsky et al. (2022b, 2024) acknowledge that impact parameter variations (TDVs) are sensitive to multiple dynamical parameters, and different combinations of inclination and nodal motion can yield similar TDV observations. Specifically, TDVs are driven by nodal precession, with the rate of change of the impact parameter given by:

$$\frac{db}{dt} = b \cdot \frac{d\Omega}{dt} \cdot \cot I \quad (27)$$

where b is the impact parameter, Ω is the longitude of the ascending node, and I is the inclination. This relationship indicates that TDVs can result from various combinations of inclination and nodal precession rates, leading to multiple plausible interpretations of the data. In systems with more planets, the complexity of interactions increases, potentially expanding the number of viable solutions. Their studies mention instances where the fitting process converged to different local minima, particularly in systems with numerous planets (e.g., KOI-834 as discussed in Judkovsky et al. (2024)). This suggests that the *dynamical fits* can yield multiple valid solutions, which may overestimate the number of significant TDVs in multi-planet systems due to the flexibility in parameter assignments to fit observed variations.

Additionally, their photodynamical model assumes that all significant gravitational interactions occur between the transiting planets. However, this approach has limitations, especially for single-planet systems. Their model cannot fit the Transit Duration Variations (TDVs) from one-planet systems because numerical simulations require interactions between multiple bodies. Yet, based on the planets selected by Shahaf et al. (2021) from Holczer et al. (2016)'s fitting, 19 KOIs are from single-planet systems but exhibit strong TDVs, likely caused by their un-transiting companions. Furthermore, planetary candidates without sufficient data to be dy-

namically constrained can have a similar effect as non-transiting companions; they might influence the orbits of planets within the system through gravitational interactions but are not included in the fitting. These unmodeled perturbations might cause the model to attribute observed variations to changes in the impact parameters of the transiting planets when, in reality, they are due to unseen companions.

Lastly, each additional planet increases the dimensionality of the parameter space by eight. Navigating this high-dimensional space becomes computationally challenging, potentially leading to inefficient sampling where some regions are inadequately explored or overexplored.

6. CONCLUSION

Our research outlines the theoretical derivation of the Log Likelihood Ratio (LLR) between the Null Model (\mathcal{M}_0), which assumes no change in the impact parameter over time, and the Alternative Model (\mathcal{M}_1), which incorporates a changing impact parameter, under the flux model posited by Mandel & Agol (2002). We then present the variation of the LLR as a function of the impact parameter rate of change, \dot{b} , for three noise levels: 30 ppm, 100 ppm, and 300 ppm. At these noise levels, the LLR reaches 20 and 50 as \dot{b} increases from 0.0037 to 0.0929. Under typical noise conditions of 100 ppm, our analysis shows that \dot{b} must exceed 0.0124 for SPIVA to detect the variation, consistent with findings that typical detectable transit impact parameter variation rates are around 10^{-2}yr^{-1} .

Furthermore, we present our methodologies for detecting changes in impact parameters from planetary transits using MCMC techniques: the *Individual Fit* and the SIPVA. We generate artificial light curves with various LLR via Monte Carlo simulations. First, we outline the parameters and likelihood function of the *Individual Fit*, which involves fitting each transit independently using MCMC and then combining the posterior estimates of the impact parameter from each transit with linear regression to estimate the impact parameter variation. We also describe the setup for SIPVA, which incorporates the assumption of linear time-dependent impact parameters within the MCMC by folding transits. We also explain the technique for quantifying inter-transit uncertainty. Finally, we evaluate the effectiveness of *Individual Fits* and SIPVA by analyzing the recovery rate and accuracy across different LLR and the areas under the ROC curve.

The bar graph in Figure 2 represents the proportion of successful recoveries. SIPVA consistently outperforms *Individual Fitting* methods across all LLR. This is further verified by the ROC curve in Figure 3, which

compares the true positive rate of each fitting method against the false positive rate. The area under the curve for SIPVA exceeds that of both *Individual Fitted* TDV and Impact Parameter. Lastly, we compare the accuracy of recovered Impact Parameter Variation using the percentage difference box plot (Figure 4). As the LLR increases, both SIPVA and *Individual Fit* demonstrate improved estimation accuracy, with decreasing percentage differences. However, SIPVA outperforms *Individual Fit* by significantly reducing percentage differences at higher LLR values despite initially showing a higher percentage difference at LLR = 10. This improved performance of SIPVA at higher LLR values is due to its assumption of a linear impact parameter change over time, which holds when the signal is strong. In contrast, at lower LLR values, where the signal is weaker, SIPVA’s linear model assumption breaks down and fits the noise, leading to larger errors. Meanwhile, *Individual Fit* remains more stable by allowing independent variation of the impact parameter for each transit, resulting in consistent but modest improvements across all LLR values.

Furthermore, we applied both individual and SIPVA methods to analyze the changes in the impact parameters of 16 planetary systems selected by Millholland et al. (2021) for exhibiting significant long-term Transit Duration Variations, using data provided by Holczer et al. (2016). The *Individual Fit* identified 4 of the 16 planets with significant trends in impact parameter changes ($t_{b,\text{ind}} > 3$), while the SIPVA detected significant long-term trends for 10 of the 16 planets ($t_{b,\text{grp}} > 3$). For all planets showing significant changes in the SIPVA, the direction of impact parameter variation was consistent with the trends observed in Transit Duration Variation fitting from Holczer et al. (2016). The SIPVA method failed to recover the impact parameter changes for four planets due to the limited number of detrended transits and the strong noise associated with each transit. Additionally, although KOIs 142.01 and 377.01 have multiple clean detrended transits, the overall trend in their impact parameter changes may not follow a simple linear pattern. In particular, KOI 142.01 exhibits a superposition of a wave-like function and a linear trend, as previously noted by Nesvorný et al. (2013).

KOI 377.02, the candidate with the highest t -score among all 16, is illustrated by the SIPVA posterior parameter estimations shown in Figure 7. The parameters in the corner plot, listed in order, are: ρ_* , the stellar density; t_e , the transit midtime, normalized to 0 from the transit folding process; T , the orbital period of the planet; b_0 , the initial impact parameter; \dot{b} , the rate of change in the impact parameter over time; p , the planet-

star area ratio; secw and sesw , which parameterize the eccentricity and orientation of the orbit; and $q1_{\text{Kepler}}$ and $q2_{\text{Kepler}}$, the quadratic limb darkening coefficients. The corner plot provides the parameter uncertainties and correlations within the model.

The SIPVA approach offers several advantages over *Individual Fitting* in recovering impact parameter variations. First, SIPVA reduces the limitations of relying heavily on prior knowledge, which is particularly beneficial for planets with shorter periods and fewer data points per transit. In *Individual Fitting*, limited data can lead to high uncertainty within the likelihood function, increasing dependency on prior information and introducing bias in parameter estimation. By aggregating all transits, SIPVA creates a more robust likelihood function with sufficient data points, thereby reducing the influence of prior assumptions. Second, SIPVA introduces a strong assumption about the time-dependent behavior of the impact parameter (linear in this paper). This assumption significantly reduces the variance in the estimates by constraining the degrees of freedom for the impact parameter across transits (from $10N_T$ parameters down to 11). Intuitively, this constraint reduces the variability of flexible parameters like the limb darkening coefficients, enhancing the recovery rate of changes in the impact parameter. In *Individual Fits*, these coefficients may vary significantly across transits due to limited data, potentially obscuring accurate signals. SIPVA, however, employs a single set of coefficients optimized to minimize the root-mean-square error across all transits, thus preserving the integrity of the time-dependent impact parameter variations in the data.

Lastly, we develop a theoretical model to estimate the relative frequency of planets exhibiting significant impact parameter changes ($\dot{b} \geq 0.01$) across all *Kepler* observations, based on the mutual inclination derivation established by Murray & Dermott (1999) and incorporating the inclination distributions derived from Zhu et al. (2018) and Fabrycky et al. (2014). Figure 6 presents the relative frequency of impact parameter variation across different planet multiplicities, while Table 3 shows the proportion and frequencies of significant cases. Contrary to the intuition that systems with more planets would exhibit larger impact parameter changes due to increased gravitational interactions, the simulations suggest that the frequency of significant \dot{b} actually decreases with higher planet multiplicity. This is attributed to the exponential decrease in inclination dispersion as the number of planets increases (Zhu et al. 2018), leading to smaller mutual inclinations and, thus, smaller \dot{b} values. Although the number of gravitational interactions grows

quadratically with the number of planets, the strength of each interaction diminishes exponentially, and perturbations from neighboring planets may cancel out, resulting in fewer significant \dot{b} occurrences in higher-multiplicity systems. From a stability standpoint, systems with more planets tend to adopt more coplanar configurations to maintain long-term dynamical stability.

Comparing our theoretical predictions with observations from [Holczer et al. \(2016\)](#), as selected by [Shahaf et al. \(2021\)](#), we find that both our simulations and their observations suggest a decreasing number of planets exhibiting significant impact parameter variations (\dot{b}) as planetary multiplicity increases. This trend is consistent with [Shahaf et al. \(2021\)](#), where significant Transit Duration Variations (TDVs) decrease in systems with more planets. Interestingly, [Holczer et al. \(2016\)](#)'s observations show significant TDVs in single-planet systems, which was unexpected since such systems lack additional planets to exert gravitational perturbations. This might suggest the presence of undetected, highly inclined companion planets causing orbital perturbations, or, less likely, by stellar oblateness inducing orbital precession. While the number of observed planets with significant TDVs is lower than our model predicts—likely due to selection biases and observational limitations—the relative proportion agrees with the decreasing trend of significant impact parameter changes as planetary multiplicity increases.

When comparing our theoretical predictions of impact parameter variations with observations from [Jud-](#)

[kovsky et al. \(2022b, 2024\)](#), we find a discrepancy: their data indicate that the relative frequency of planets exhibiting significant impact parameter changes increases with the number of planets in a system, which contrasts with other studies ([Zhu et al. 2018](#); [Holczer et al. 2016](#); [Becker & Adams 2015](#)) showing a decreasing trend with higher planetary multiplicity. We propose that this inconsistency may result from potential overfitting in their dynamical models, particularly in multi-planet systems where additional planets often have weaker signals and contribute less new information, leading to parameter stretching and unusually high eccentricities. As more planets are included, parameters like eccentricities and inclinations can become interdependent, complicating the unique determination of each planet's properties and allowing multiple valid solutions that might overestimate significant Transit Duration Variations (TDVs). Moreover, their model assumes gravitational interactions are only among transiting planets, which misses the impact of non-transiting companions—especially in single-planet systems where TDVs may be caused by unseen planets. Lastly, the increasing dimensionality of the parameter space with each added planet makes the computational process more challenging, potentially leading to inefficient sampling and fitting issues and contributing to the observed discrepancy.

ACKNOWLEDGMENTS

We thank Xian-Yu Wang for insightful discussions about modeling strategies.

APPENDIX

A. DERIVATION OF THE RELATIONSHIP BETWEEN LLR AND IMPACT PARAMETER VARIATION T-SCORE

We denote the Null Hypothesis (\mathcal{M}_0) as the model without considering impact parameter variation (i.e., $\dot{b} = 0$), and the Alternative Hypothesis (\mathcal{M}_1) as the model that accounts for impact parameter variation (i.e., $\dot{b} \neq 0$). The likelihood ratio Λ is defined as:

$$\Lambda = \frac{\sup_{\vec{\Theta}, b_0 \in \mathcal{M}_0} \mathcal{L}(\vec{\Theta}, b_0)}{\sup_{\vec{\Theta}, b_0, \dot{b} \in \mathcal{M}_1} \mathcal{L}(\vec{\Theta}, b_0, \dot{b})} \quad (\text{A1})$$

The test statistic λ is then:

$$\lambda = -2 \log \Lambda = -2 \left(\log \mathcal{L}(\vec{\Theta}_0, \hat{b}_0) - \log \mathcal{L}(\vec{\Theta}_1, \hat{b}_0, \hat{\dot{b}}) \right) \quad (\text{A2})$$

where $(\vec{\Theta}_0, \hat{b}_0)$ are the maximum likelihood estimates (MLEs) under \mathcal{M}_0 , and $(\vec{\Theta}_1, \hat{b}_0, \hat{\dot{b}})$ are the MLEs under \mathcal{M}_1 . The degrees of freedom (df) for the chi-squared distribution of λ is:

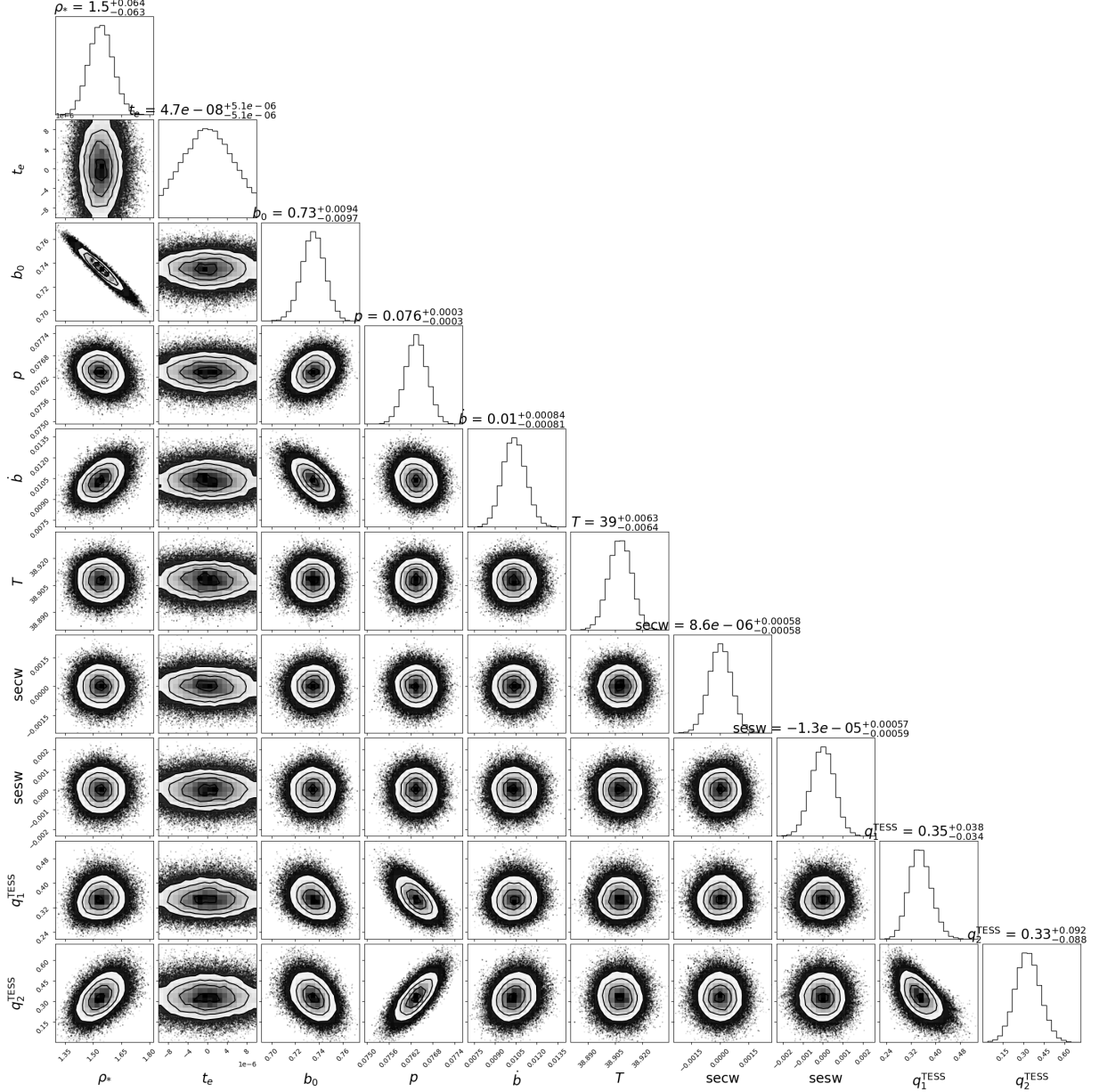


Figure 7. Corner plot of the posterior parameter estimations from SIPVA for KOI 377.02, which has the highest t-score among all 16 candidates identified by Millholland et al. (2021). The parameters shown are ρ_* , the stellar density; t_e , the transit midtime, normalized to 0 from the transit folding process; T , the orbital period of the planet; b_0 , the initial impact parameter; \dot{b} , the rate of change in the impact parameter over time; p , the planet-star area ratio; secw and sesw , which parameterize the eccentricity and orientation of the orbit; and $q_{1\text{Kepler}}$ and $q_{2\text{Kepler}}$, the quadratic limb darkening coefficients.

$$df = \left| \vec{\Theta}, b_0, \dot{b} \right| - \left| \vec{\Theta}, b_0 \right| = 1 \quad (\text{A3})$$

since \mathcal{M}_1 has one additional parameter (\dot{b}) compared to \mathcal{M}_0 . The difference in log-likelihoods is:

$$\Delta\mathcal{L} = \mathcal{L}(\vec{\Theta}_1, \hat{b}_0, \hat{\dot{b}}) - \mathcal{L}(\vec{\Theta}_0, \hat{b}_0) \quad (\text{A4})$$

Assuming that $\hat{\dot{b}}$ is small and $\vec{\Theta}_1 \approx \vec{\Theta}_0$ (since the inclusion of \dot{b} does not significantly change the estimates of other parameters for small \dot{b}), we can write:

$$\Delta\mathcal{L} \approx \mathcal{L}(\vec{\Theta}_0, \hat{b}_0, \hat{b}) - \mathcal{L}(\vec{\Theta}_0, \hat{b}_0) \quad (\text{A5})$$

Using the Taylor expansion:

$$\Delta\mathcal{L} \approx \hat{b} \frac{\partial\mathcal{L}}{\partial\hat{b}} \Big|_{\hat{b}=0} + \frac{1}{2} \hat{b}^2 \frac{\partial^2\mathcal{L}}{\partial\hat{b}^2} \Big|_{\hat{b}=0} \quad (\text{A6})$$

But under the null hypothesis, the score function (first derivative) evaluated at $\hat{b} = 0$ is zero:

$$\frac{\partial\mathcal{L}}{\partial\hat{b}} \Big|_{\hat{b}=0} = 0 \quad (\text{A7})$$

Therefore:

$$\Delta\mathcal{L} \approx \frac{1}{2} \hat{b}^2 \frac{\partial^2\mathcal{L}}{\partial\hat{b}^2} \Big|_{\hat{b}=0} \quad (\text{A8})$$

The negative of the second derivative of the log-likelihood to \hat{b} evaluated at $\hat{b} = 0$ is the observed Fisher information $I_{\hat{b}\hat{b}}$:

$$I_{\hat{b}\hat{b}} = - \frac{\partial^2\mathcal{L}}{\partial\hat{b}^2} \Big|_{\hat{b}=0} \quad (\text{A9})$$

Substituting back into $\Delta\mathcal{L}$:

$$\Delta\mathcal{L} \approx -\frac{1}{2} \hat{b}^2 I_{\hat{b}\hat{b}} \quad (\text{A10})$$

The test statistic λ becomes:

$$\lambda = -2\Delta\mathcal{L} = -2 \left(\mathcal{L}(\vec{\Theta}_1, \hat{b}_0, \hat{b}) - \mathcal{L}(\vec{\Theta}_0, \hat{b}_0) \right) \approx \hat{b}^2 I_{\hat{b}\hat{b}} \quad (\text{A11})$$

The t-score for \hat{b} is defined as:

$$t = \frac{\hat{b} - 0}{\text{SE}(\hat{b})} = \hat{b} \times \left(\frac{1}{\text{SE}(\hat{b})} \right) \quad (\text{A12})$$

But the standard error $\text{SE}(\hat{b})$ is related to the Fisher information:

$$\text{SE}(\hat{b}) = \frac{1}{\sqrt{I_{\hat{b}\hat{b}}}} \quad (\text{A13})$$

Therefore, we have $t^2 = \hat{b}^2 I_{\hat{b}\hat{b}}$, which proves $\lambda \approx t^2$, where, in our context, the test statistic λ is the Log-Likelihood Ratio (LLR).

REFERENCES

- Agol, E., & Deck, K. 2016a, TTVFaster: First order eccentricity transit timing variations (TTVs), Astrophysics Source Code Library, record ascl:1604.012
- . 2016b, ApJ, 818, 177, doi: [10.3847/0004-637X/818/2/177](https://doi.org/10.3847/0004-637X/818/2/177)
- Agol, E., & Fabrycky, D. C. 2018, Transit-Timing and Duration Variations for the Discovery and Characterization of Exoplanets (Springer International Publishing), 797–816, doi: [10.1007/978-3-319-55333-7-7](https://doi.org/10.1007/978-3-319-55333-7-7)
- Agol, E., Steffen, J., Sari, R., & Clarkson, W. 2005, MNRAS, 359, 567, doi: [10.1111/j.1365-2966.2005.08922.x](https://doi.org/10.1111/j.1365-2966.2005.08922.x)
- Becker, J. C., & Adams, F. C. 2015, Monthly Notices of the Royal Astronomical Society. <https://arxiv.org/abs/1511.00009>
- Carter, J. A., Agol, E., Chaplin, W. J., et al. 2012, Science, 337, 556, doi: [10.1126/science.1223269](https://doi.org/10.1126/science.1223269)

- Castelli, F., & Kurucz, R. L. 2003, in IAU Symposium, Vol. 210, Modelling of Stellar Atmospheres, ed. N. Piskunov, W. W. Weiss, & D. F. Gray, A20, doi: [10.48550/arXiv.astro-ph/0405087](https://doi.org/10.48550/arXiv.astro-ph/0405087)
- Chambers, J. E. 1999, MNRAS, 304, 793, doi: [10.1046/j.1365-8711.1999.02379.x](https://doi.org/10.1046/j.1365-8711.1999.02379.x)
- Claret, A., & Bloemen, S. 2011, Astronomy & Astrophysics, 529, A75, doi: [10.1051/0004-6361/201116451](https://doi.org/10.1051/0004-6361/201116451)
- Dai, F., Masuda, K., Beard, C., et al. 2023, AJ, 165, 33, doi: [10.3847/1538-3881/aca327](https://doi.org/10.3847/1538-3881/aca327)
- Deck, K. M., Agol, E., Holman, M. J., & Nesvorný, D. 2014, The Astrophysical Journal, 787, 132, doi: [10.1088/0004-637x/787/2/132](https://doi.org/10.1088/0004-637x/787/2/132)
- Doyle, L. R., Carter, J. A., Fabrycky, D. C., et al. 2011, Science, 333, 1602, doi: [10.1126/science.1210923](https://doi.org/10.1126/science.1210923)
- Fabrycky, D. C., Lissauer, J. J., Ragozzine, D., et al. 2014, ApJ, 790, 146, doi: [10.1088/0004-637X/790/2/146](https://doi.org/10.1088/0004-637X/790/2/146)
- Fang, J., & Margot, J.-L. 2012, ApJ, 761, 92, doi: [10.1088/0004-637X/761/2/92](https://doi.org/10.1088/0004-637X/761/2/92)
- Foreman-Mackey, D. 2018, kplr: Tools for working with Kepler data using Python, Astrophysics Source Code Library, record ascl:1807.027. <http://ascl.net/1807.027>
- Foreman-Mackey, D., Hogg, D. W., Lang, D., & Goodman, J. 2013, Publications of the Astronomical Society of the Pacific, 125, 306–312, doi: [10.1086/670067](https://doi.org/10.1086/670067)
- Gilliland, R. L., Chaplin, W. J., Jenkins, J. M., Ramsey, L. W., & Smith, J. C. 2015, AJ, 150, 133, doi: [10.1088/0004-6256/150/4/133](https://doi.org/10.1088/0004-6256/150/4/133)
- Grimm, S. L., Demory, B.-O., Gillon, M., et al. 2018, A&A, 613, A68, doi: [10.1051/0004-6361/201732233](https://doi.org/10.1051/0004-6361/201732233)
- Hadden, S., & Lithwick, Y. 2017, AJ, 154, 5, doi: [10.3847/1538-3881/aa71ef](https://doi.org/10.3847/1538-3881/aa71ef)
- Holzner, T., Mazeh, T., Nachmani, G., et al. 2016, The Astrophysical Journal Supplement Series, 225, 9, doi: [10.3847/0067-0049/225/1/9](https://doi.org/10.3847/0067-0049/225/1/9)
- Javaheri, P., Rein, H., & Tamayo, D. 2023, The Open Journal of Astrophysics, 6, doi: [10.21105/astro.2307.05683](https://doi.org/10.21105/astro.2307.05683)
- Jones, D., Ragozzine, D., & Fabrycky, D. 2022, in Bulletin of the American Astronomical Society, Vol. 54, 102.360
- Judkovsky, Y., Ofir, A., & Aharonson, O. 2020, The Astronomical Journal, 160, 195, doi: [10.3847/1538-3881/abb406](https://doi.org/10.3847/1538-3881/abb406)
- . 2022a, The Astronomical Journal, 163, 90, doi: [10.3847/1538-3881/ac3d95](https://doi.org/10.3847/1538-3881/ac3d95)
- . 2022b, The Astronomical Journal, 163, 91, doi: [10.3847/1538-3881/ac3d96](https://doi.org/10.3847/1538-3881/ac3d96)
- . 2024, The Astronomical Journal, 167, 103, doi: [10.3847/1538-3881/ad16e2](https://doi.org/10.3847/1538-3881/ad16e2)
- Kipping, D. M. 2010, Monthly Notices of the Royal Astronomical Society, 408, 1758–1769, doi: [10.1111/j.1365-2966.2010.17242.x](https://doi.org/10.1111/j.1365-2966.2010.17242.x)
- Langford, Z., & Agol, E. 2024, A differentiable N-body code for transit timing and dynamical modelling – II. Photodynamics. <https://arxiv.org/abs/2410.03874>
- Li, G., Dai, F., & Becker, J. 2020, The Astrophysical Journal Letters, 890, L31, doi: [10.3847/2041-8213/ab72f4](https://doi.org/10.3847/2041-8213/ab72f4)
- Lightkurve Collaboration, Cardoso, J. V. d. M., Hedges, C., et al. 2018, Lightkurve: Kepler and TESS time series analysis in Python, Astrophysics Source Code Library. <http://ascl.net/1812.013>
- Lissauer, J. J., Ragozzine, D., Fabrycky, D. C., et al. 2011, ApJS, 197, 8, doi: [10.1088/0067-0049/197/1/8](https://doi.org/10.1088/0067-0049/197/1/8)
- Lithwick, Y., Xie, J., & Wu, Y. 2012, ApJ, 761, 122, doi: [10.1088/0004-637X/761/2/122](https://doi.org/10.1088/0004-637X/761/2/122)
- Lithwick, Y., Xie, J., & Wu, Y. 2012, The Astrophysical Journal, 761, 122, doi: [10.1088/0004-637x/761/2/122](https://doi.org/10.1088/0004-637x/761/2/122)
- Mandel, K., & Agol, E. 2002, The Astrophysical Journal, 580, L171, doi: [10.1086/345520](https://doi.org/10.1086/345520)
- Masuda, K. 2022, pykepler: Python Tools for Analyzing Kepler Data, <https://github.com/kemasuda/pykepler>, GitHub
- Masuda, K., Libby-Roberts, J. E., Livingston, J. H., et al. 2024, arXiv e-prints, arXiv:2410.01625, doi: [10.48550/arXiv.2410.01625](https://doi.org/10.48550/arXiv.2410.01625)
- Millholland, S. C., He, M. Y., Ford, E. B., et al. 2021, AJ, 162, 166, doi: [10.3847/1538-3881/ac0f7a](https://doi.org/10.3847/1538-3881/ac0f7a)
- Moon, B., Jeong, D.-G., Oh, S., & Sohn, J. 2017, Journal of Astronomy and Space Sciences, 34, 99, doi: [10.5140/JASS.2017.34.2.99](https://doi.org/10.5140/JASS.2017.34.2.99)
- Murray, C. D., & Dermott, S. F. 1999, Solar System Dynamics, 1st edn. (Cambridge, UK: Cambridge University Press), doi: [10.1017/CBO9781139174817](https://doi.org/10.1017/CBO9781139174817)
- Nesvorný, D., & Beaugé, C. 2010, The Astrophysical Journal, 709, L44–L48, doi: [10.1088/2041-8205/709/1/144](https://doi.org/10.1088/2041-8205/709/1/144)
- Nesvorný, D., Kipping, D., Terrell, D., et al. 2013, The Astrophysical Journal, 777, 3, doi: [10.1088/0004-637x/777/1/3](https://doi.org/10.1088/0004-637x/777/1/3)
- Parviainen, H. 2015, Monthly Notices of the Royal Astronomical Society, 450, 3233, doi: [10.1093/mnras/stv894](https://doi.org/10.1093/mnras/stv894)
- Rein, H., & Liu, S. F. 2012, A&A, 537, A128, doi: [10.1051/0004-6361/201118085](https://doi.org/10.1051/0004-6361/201118085)
- Rein, H., & Spiegel, D. S. 2014, Monthly Notices of the Royal Astronomical Society, 446, 1424–1437, doi: [10.1093/mnras/stu2164](https://doi.org/10.1093/mnras/stu2164)
- Rein, H., & Tamayo, D. 2015, MNRAS, 452, 376, doi: [10.1093/mnras/stv1257](https://doi.org/10.1093/mnras/stv1257)

- Rein, H., Tamayo, D., & Brown, G. 2019a, *Monthly Notices of the Royal Astronomical Society*, 489, 4632–4640, doi: [10.1093/mnras/stz2503](https://doi.org/10.1093/mnras/stz2503)
- Rein, H., Hernandez, D. M., Tamayo, D., et al. 2019b, *Monthly Notices of the Royal Astronomical Society*, 485, 5490–5497, doi: [10.1093/mnras/stz769](https://doi.org/10.1093/mnras/stz769)
- Shahaf, S., Mazeh, T., Zucker, S., & Fabrycky, D. 2021, *Monthly Notices of the Royal Astronomical Society*, 505, 1293, doi: [10.1093/mnras/stab1359](https://doi.org/10.1093/mnras/stab1359)
- Sing, D. K. 2010, *Astronomy and Astrophysics*, 510, A21, doi: [10.1051/0004-6361/200913675](https://doi.org/10.1051/0004-6361/200913675)
- Tremaine, S., & Dong, S. 2012, *AJ*, 143, 94, doi: [10.1088/0004-6256/143/4/94](https://doi.org/10.1088/0004-6256/143/4/94)
- Van Eylen, V., & Kjelksen, H. 2014, arXiv preprint arXiv:1403.1372, <https://ar5iv.labs.arxiv.org/html/1403.1372>
- Wisdom, J., & Holman, M. 1991, *AJ*, 102, 1528, doi: [10.1086/115978](https://doi.org/10.1086/115978)
- Yoffe, G., Ofir, A., & Aharonson, O. 2021, *ApJ*, 908, 114, doi: [10.3847/1538-4357/abc87a](https://doi.org/10.3847/1538-4357/abc87a)
- Zhu, W., Petrovich, C., Wu, Y., Dong, S., & Xie, J. 2018, *ApJ*, 860, 101, doi: [10.3847/1538-4357/aac6d5](https://doi.org/10.3847/1538-4357/aac6d5)